Raman Spectrum of Diamond*

S. A. Solin† and A. K. Ramdas
Department of Physics, Purdue University, Lafayette, Indiana 47907
(Received 30 September 1969)

The first- and second-order Raman spectra of diamond were studied using the 4880 Å and 5145 Å lines of an Ar ion laser and the 6328 Å line of a He-Ne laser. The spectra were recorded at room, liquid-nitrogen, and liquid-helium temperatures. In addition to the second-order spectrum previously reported by Krishnan, a new weaker second-order spectrum was observed in the range 1600–2100 cm^{-1}. Polarization studies were carried out on both the first- and second-order spectra. From such studies it was established that the 1332-cm^{-1} Raman line is the zone-center optical phonon with $\Gamma^{(25+)}$ (F_{2g}) symmetry. The prominent features in both the second-order Raman spectra reported here and the second-order infrared spectra are interpreted in terms of the critical points of the phonon dispersion curves established from neutron spectroscopy and on the basis of space-group selection rules.

I. INTRODUCTION

THE lattice dynamics of diamond has attracted considerable attention since the data on its specific heat were cited by Einstein[1] in support of his theory of the specific heat of solids. Infrared absorption,[2–4] Raman effect,[5,6] and inelastic neutron scattering,[7,8] all of which can be used in the study of the lattice dynamics of crystals, have since been investigated for this material. Though a complete set of dispersion curves can be obtained from inelastic neutron scattering, at present the accuracy of phonon energies deduced from such measurements does not compare with that of infrared absorption or Raman scattering. On the other hand, a critical-point analysis of the infrared absorption and Raman spectrum is difficult to carry out in the absence of neutron-scattering data. It should also be noted that the symmetry of the phonons at various points in the Brillouin zone cannot be determined by neutron spectroscopy. Hardy and Smith[3] performed a critical-point analysis of the second-order infrared absorption spectrum, whereas Johnson and Loudon[9] and Bilz *et al.*[10] used both infrared and Raman spectra. The above studies were carried out before neutron-scattering data became available. Warren and co-workers,[7] who reported the neutron-scattering experiments, attempted to explain the infrared data of Hardy and Smith[3] but did not make use of the available Raman spectrum. It is clearly of interest to interpret the results of all three types of measurement in a self-consistent manner. In this context, a study of the polarization characteristics and the temperature dependence of the second-order Raman spectrum should be particularly valuable. The previous measurements of Krishnan,[11] Narayanan,[12] and Raman[6] did not touch upon these aspects. Also, in their work, the 2537 Å Hg resonance radiation used to excite the Raman spectrum was accompanied by mercury lines which obscured parts of the second-order spectrum. The limitations of the photographic technique used precluded the observation of subtle features in the second-order spectrum. The purpose of this paper is to present the results of a detailed study of the polarization characteristics and temperature dependence of the first- and second-order Raman spectrum of diamond obtained with laser excitation, oriented samples, and photoelectric detection.[13]

II. EXPERIMENTAL

The Raman spectra were excited with either the 4880 or the 5145 Å radiation from an Ar^+ laser,[14] or the 6328 Å radiation from a He-Ne laser.[15] Figure 1 shows the block diagram of the Raman spectrometer. Radiation from the Ar^+ laser is introduced into the system by removing M_2. Most of the arrangement used is typical of systems currently employed in right-angle

* Work supported by the Advanced Research Projects Agency and the National Science Foundation.
† Present address: The James Franck Institute, The University of Chicago, Chicago, Ill.
[1] A. Einstein, Ann. Physik **22**, 180 (1907).
[2] The infrared absorption spectrum of diamond has been extensively studied by many investigators since the early work of R. Robertson, J. J. Fox, and A. E. Martin, Phil. Trans. Roy. Soc. London **A232**, 463 (1934). See, for example, K. G. Ramanathan, Proc. Indian Acad. Sci. Sect. A **24**, 137 (1946); G. B. B. M. Sutherland, D. E. Blackwell, and W. G. Simeral, Nature **174**, 901 (1954); R. J. Collins and H. Y. Fan, Phys. Rev. **97**, 39 (1955); W. Kaiser and W. L. Bond, *ibid.* **115**, 857 (1959), C. V. Raman, Proc. Indian Acad. Sci. Sect. A **55**, 1 (1962). See also Refs. 3 and 4.
[3] J. R. Hardy and S. D. Smith, Phil. Mag. **6**, 1163 (1961).
[4] R. Wehner, H. Borik, W. Kress, A. R. Goodwin, and S. D. Smith, Solid State Commun. **5**, 307 (1967).
[5] See D. Krishnamurti, Proc. Indian Acad. Sci. Sect. A **40**, 211 (1954) for a complete bibilography up to 1954.
[6] C. V. Raman, Proc. Indian Acad. Sci. Sect. A **44**, 99 (1956).
[7] J. L. Warren, J. L. Yarnell, G. Dolling, and R. A. Cowley, Phys. Rev. **158**, 805 (1966); J. L. Warren, R. G. Wenzel, and J. L. Yarnell, in *Inelastic Scattering of Neutrons* (International Atomic Energy Agency, Vienna, 1965), Vol. I, p. 361.
[8] G. Peckham, Solid State Commun. **5**, 311 (1967).
[9] F. A. Johnson and R. Loudon, Proc. Roy. Soc. (London) **A281**, 274 (1964). See also F. A. Johnson, in *Progress in Semiconductors*, edited by A. F. Gibson and R. E. Burgess (Temple Press Books, Ltd., London, 1965), Vol. 9, p. 179.
[10] H. Bilz, R. Geick, and K. F. Renck, in *Lattice Dynamics*, edited by R. F. Wallis (Pergamon Press, Ltd., London, 1965), p. 355.
[11] R. S. Krishnan, Proc. Indian Acad. Sci. Sect. A **26**, 399 (1947). Earlier work by this author is referred to in this paper.
[12] P. S. Narayanan, Proc. Indian Acad. Sci. Sect. A **32**, 1 (1950).
[13] A preliminary report on this work was presented in Bull. Am. Phys. Soc. **14**, 342 (1969).
[14] Model 52A, Coherent Radiation Laboratories, 932 East Meadow Dr., Palo Alto, Calif., 94303.
[15] Model 125, Spectra Physics, 1255 Terra Bella Ave., Mountain View, Calif. 94040.

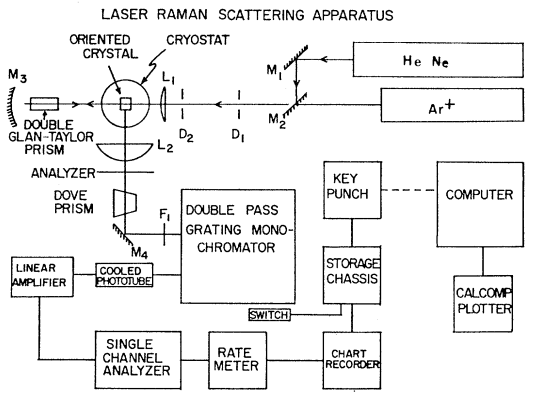

FIG. 1. Block diagram of right-angle Raman-scattering apparatus. D_1 and D_2 are adjustable diaphragms; M_1 and M_2 are dielectric coated, and M_3 and M_4 are aluminized-front-surface mirrors.

Raman scattering experiments. The following are the additional features: (i) The laser beam was both multipassed and focused in the sample. This was achieved by forming a cavity between a spherical mirror M_3 and the plane surface of the laser output mirror. The double Glan-Taylor prism was inserted between the sample and M_3 in order to ensure that the light incident on the sample remains linearly polarized after reflection from the aluminized surface of M_3. (ii) The data, in addition to being displayed on a chart recorder, were simultaneously and automatically punched onto computer cards for processing. A computer program was written which corrected the data for all dispersive effects included in the transfer function of the spectrometer.[16] The instrumental transfer function for light linearly polarized parallel and perpendicular to the grating grooves was determined for each set of conditions encountered in a given Raman measurement by observing the response of the entire system to a "blackbody" source and correcting it for the known spectral output of the source. Having corrected the data for the instrumental transfer function, the computer produces a plot of the intensity of the Raman spectrum in arbitrary units versus wave number shift $\tilde{\nu}$ prepared by a Calcomp[17]-model 563-digital incremental plotter. The computer program also made provision for the plotting of both the first and second-derivative of the Raman intensity with respect to $\tilde{\nu}$. These derivative plots were particularly useful for locating critical points in the second-order Raman spectrum.

The optical cryostat used has been described elsewhere[18]; it has been modified by the addition of a third window for use in right-angle Raman scattering experiments. Measurements at low temperatures were made with liquid helium and liquid nitrogen as coolants; with these, sample temperatures $\sim$20 and 80°K, respectively, were obtained. A Perkin-Elmer model E-1 monochromator[19] used in the double-pass mode together with various Corning glass filters (F_1 in Fig. 1) provided adequate stray-light characteristics in the region of interest.

In the course of the work reported here, a wide variety of diamonds[20] were examined; viz., natural type I, IIa, IIb, and synthetic type IIb. The first-order Raman line was observed with all of these. Depolarization measurements were made on two South African type-IIb samples cut in the form of rectangular parallelepipeds 2×2×5 mm and optically polished on all six faces, these faces being (001), (110), and (1$\bar{1}$0) for sample D1 and (111), (1$\bar{1}$0), ($\bar{1}\bar{1}$2) for the other, D2. The second-order spectrum was extensively studied using D1 which was free from luminescence in the range in which the first- and second-order spectra excited by the Ar+ laser occurred. All spectra reported in this paper were obtained from sample D1 unless otherwise specified. Luminescence posed a serious problem for the observation of the second-order Raman spectrum in many of the samples examined, the problem being most severe in the case of synthetic type-IIb samples. However, even in specimens which exhibited strong luminescence in the region of interest, the second-order Raman spectrum could be observed superposed on it.

TABLE I. Depolarization of the 1332-cm^{-1} Raman line.

Depolarization ratio[a]	Theory	Experiment
$\rho_1=\dfrac{I_{Z'(X'Z')Y'}}{I_{Z'(X'X')Y'}}$	$\dfrac{d^2}{d^2}=1$	0.93
$\rho_2=\dfrac{I_{Y'(Z'Y')X'}}{I_{Y'(Z'Z')X'}}$	$\dfrac{d^2}{0}=\infty$	23.2
$\rho_3=\dfrac{I_{Z'(Y'Z')Y'}}{I_{Z'(Y'X')Y'}}$	$\dfrac{d^2}{0}=\infty$	10.4
ρ_4[b]$=\dfrac{I_{Z'(X'Z'+Y'Z')Y'}}{I_{Z'(X'X'+Y'X')Y'}}$	$\dfrac{2d^2}{d^2}=2$	2.01

[a] Note $X'\|[110]$, $Y'\|[1\bar{1}0]$, $Z'\|[001]$. The measurements ρ_1, ρ_3 and ρ_4 were made with 6328-Å He-Ne line and ρ_2 with the 4880 Å Ar+ line.

[b] This corresponds to the case in which the incident light is "natural" or unpolarized. The experiment was carried out by using incident plane-polarized light with its electric vector at 45° to the scattering plane; it can be shown that the results are the same as for unpolarized light.

[16] S. A. Solin, Ph.D. thesis, Purdue University, 1970 (unpublished).

[17] California Computers Inc., Anaheim, Calif.

[18] P. Fisher, W. H. Haak, E. J. Johnson, and A. K. Ramdas, in *Proceedings of the Eighth Symposium on the Art of Glassblowing* (The American Scientific Glassblowing Society, Wilmington, Delaware, 1963), p. 136.

[19] Perkin Elmer Corporation, Norwalk, Conn.

[20] The authors are grateful to Dr. L. Du Preez, Diamond Research Laboratory, Industrial Distributors (1946) Ltd., Johannesburg, South Africa for the loan of two high-quality natural type-IIb specimens. Thanks are also due to Dr. P. Sorokin of the IBM Corporation for several natural type-I diamonds, to Dr. R. H. Wentorf of General Electric Company for many synthetic type-IIb diamonds, to Dr. E. C. Lightowlers of King's College, London, England and to Dr. E. R. Czerlinsky of the Cambridge Research Laboratories, Bedford, Massachusetts for the loan of type-IIb diamonds.

III. RESULTS AND DISCUSSION

A. First-Order Raman Spectrum

Diamond belongs to the space group O_h^7 with two atoms per primitive cell; it is well known[21] that it possesses one triply degenerate zone-center optical phonon with $\Gamma^{(25+)}$ (F_{2g}) symmetry.[22] This is the only mode which is Raman-active in the first order. The corresponding Raman line was first observed by Ramaswamy[23] who reported a single prominent line with a shift of $\sim$1332 cm^{-1} at room temperature. This shift is consistent with the phonon-dispersion curves for diamond determined by Warren *et al.*[7] The temperature dependence of the position and half-width of this line has been studied by Nayar[24] and Krishnan.[25] The previous observations[26] of its polarization characteristics are conflicting and do not agree with theoretical predictions.[27] The major source of these discrepancies appears to be a failure to take into account the anisotropy of the polarizations characteristic of degenerate Raman active modes even in cubic crystals.

The polarizability tensors corresponding to the $\Gamma^{(25+)}$ irreducible representation are[28]

$$\begin{pmatrix}0&0&0\\0&0&d\\0&d&0\end{pmatrix},\quad \begin{pmatrix}0&0&d\\0&0&0\\d&0&0\end{pmatrix},\quad \text{and}\quad \begin{pmatrix}0&d&0\\d&0&0\\0&0&0\end{pmatrix},$$

referred to the cubic axes, [100], [010], and [001]; when transformed to the axes $X'\|[110]$, $Y'\|[1\bar{1}0]$, and $Z'\|[001]$ used in the present studies these become

$$\begin{pmatrix}0&0&d/\sqrt{2}\\0&0&d/\sqrt{2}\\d/\sqrt{2}&d/\sqrt{2}&0\end{pmatrix},\quad \begin{pmatrix}0&0&d/\sqrt{2}\\0&0&-d/\sqrt{2}\\d/\sqrt{2}&-d/\sqrt{2}&0\end{pmatrix},$$

and

$$\begin{pmatrix}d&0&0\\0&-d&0\\0&0&0\end{pmatrix}.$$

The depolarization ratios are tabulated in Table I for various values of intensities $I_{i(jk)l}$ where the incident light is along i and polarized along j, scattered along l, and analyzed for k. Some of the experimental results of the polarization studies in the present investigation are shown in Fig. 2 for $Z'(X'Z')Y'$, $Z'(X'X')Y'$, $Z'(Y'Z')Y'$, and $Z'(Y'X')Y'$. It can be seen from Table I that the experimental determinations of the depolarization ratios ρ_1 and ρ_4 agree very well with the theoretical predictions. The experimental values for ρ_2 and ρ_3 are also in good agreement with those expected when the finite convergence of the scattered beam is taken into account; these values were indeed observed to increase when this convergence was decreased by stopping down the collection aperture. In view of the comparable intensities for the two polarizations leading to ρ_1 and ρ_4, the errors due to convergence were not serious. Depolarization studies performed on specimen D2 also yielded results which were in good agreement with values of ρ expected for light incident along $\langle 111\rangle$.[27]

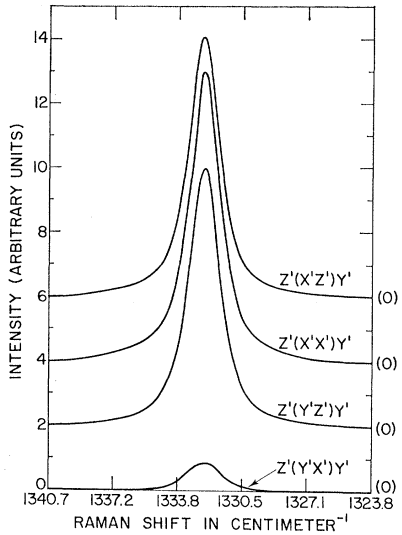

FIG. 2. Polarization features of the first-order Raman line of diamond exhibiting the tensor components $\alpha_{X'Z'}$, $\alpha_{X'X'}$, $\alpha_{Y'Z'}$, and $\alpha_{Y'X'}$; X', Y', and Z' are along [110], [1$\bar{1}$0], and [001], respectively. The spectra have been displaced vertically with respect to one another for clarity. The relative intensity scales, the zeros of which are indicated at the right of the figure, are identical for the four spectra displayed. These spectra were excited with the 6328 Å radiation of a He-Ne laser and recorded at 300°K. The abcissa is linear in wavelength rather than in wave-number shift.

The observed position and the linewidth of the first-order Raman line are presented in Table II as a function of temperature. These measurements were made with the 6328 Å radiation of the He-Ne laser and an experimentally measured spectral slitwidth of 0.40 cm^{-1}. No attempt has been made to take into account the influence of the spectral slit width on the linewidth. With

TABLE II. Temperature dependence of the half-width and shift of the first-order Raman line of diamond.

T°K	Line position (cm^{-1})	Half-width (cm^{-1})
14.9	1333.3±0.5	1.48±0.02
78.8	1333.3±0.5	1.48±0.02
202.5	1333.0±0.5	1.58±0.02
300	1332.5±0.5	1.65±0.02

[21] See, for example, S. Bhagavantam and T. Venkatarayudu, *Theory of Groups and Its Application to Physical Problems* (Andhra University, Waltair, India, 1962), p. 156.

[22] The notation for the irreducible representations of the space group O_h^7 follows J. L. Birman, Phys. Rev. **127**, 1093 (1962). Note that $\Gamma^{(25+)} \equiv F_{2g}$.

[23] C. Ramaswamy, Indian J. Phys. **5**, 97 (1930). See also C. Ramasway, Nature **125**, 704 (1930); R. Robertson and J. J. Fox, *ibid.* **125**, 704 (1930).

[24] P. G. N. Nayar, Proc. Indian Acad. Sci. Sect. A **13**, 284 (1941).

[25] R. S. Krishnan, Proc. Indian Acad. Sci. Sect. A **24**, 45 (1946).

[26] A. Mani, Proc. Indian Acad. Sci. Sect. A **20**, 117 (1944).

[27] L. Couture and J. P. Mathieu, Ann. Phys. (N. Y.) **3**, 521 (1948).

[28] R. Loudon, Advan. Phys. **13**, 423 (1964).

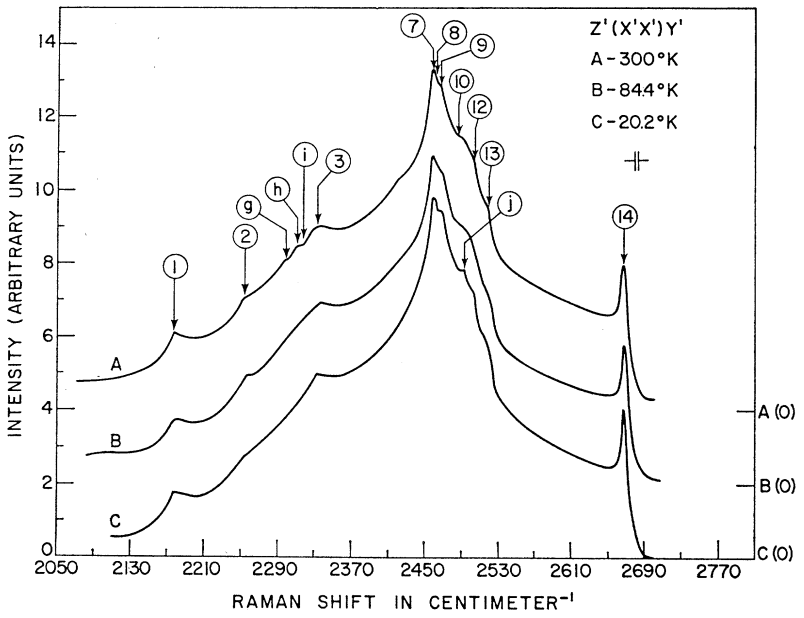

FIG. 3. Temperature dependence of the second-order Raman spectrum of diamond for $Z'(X'X')Y'$ scattering in the 2050–2770-cm^{-1} region. The spectra are displaced vertically with respect to one another for clarity. The relative intensity scales of curves A, B, and C are identical and $A(0)$, $B(0)$, $C(0)$ denote the base lines of A, B, and C, respectively. The spectra were excited with 4880 Å radiation of the Ar^+ laser.

decreasing temperature, the linewidth decreases, and the shift increases slightly, such changes being small below liquid-nitrogen temperature. Krishnan[25] has reported measurements of line positions for temperatures between 85 and 976°K which show a monotonic decrease of the Raman shift with increasing temperature. Where the present measurements overlap with his, the agreement is reasonable. Krishnan has also reported linewidths for temperatures between 300 and 970°K, and has noticed that the half-width increases with increasing temperature. The half-width of 1.65±0.02 cm^{-1} observed in the present work agrees well with his 300°K value of 1.7 cm^{-1}.

Mention should be made here of observations of the first-order Raman effect on a synthetic type-IIb diamond. The specimen was inadvertently heated to very high temperatures as a result of the absorption of the intense 5145 Å radiation of the argon laser focused on the sample and poor heat dissipation. The first-order Raman line was observed to have a shift and half-width of 1311.5±0.5 and 4.58±0.03 cm^{-1}, respectively. Using the data of Krishnan, it is estimated that the sample temperature was ≈1200°K during the measurement.

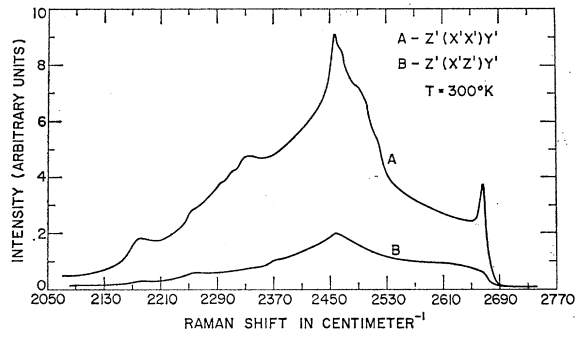

FIG. 4. Comparison of the room-temperature intensity of the second-order Raman scattering in diamond for light incident along [001], scattered along [1$\bar{1}$0] and analyzed perpendicular (curve A) and parallel (curve B) to the scattering plane. A and B are displayed with the same relative intensity scale and baseline. The spectra were excited with the 4880 Å radiation of the Ar^+ laser.

B. Second-Raman Spectrum

The second-order Raman spectrum of diamond with shifts in the range 2050–2770 cm^{-1} is shown in Fig. 3 for $Z'(X'X')Y'$ and at 300, 84.4, and 20.2°K, where X', Y', and Z' are along the same crystallographic directions as in Fig. 2. That this is indeed a Raman spectrum has been verified by exciting it with both the 4880 and 5145 Å lines of the Ar^+ laser. The cutoff at ∼2667cm^{-1} is to be expected for the second-order spectrum, since neutron spectroscopy has established that the zone-center optical phonon corresponding to the 1332-cm^{-1} first-order line is the one which has the maximum energy in the Brillouin zone. The observed Raman spectrum consists of a quasicontinuous background upon which are superimposed slope discontinuities and peaks. The intensity of the largest peak at 2458 cm^{-1} is ∼250 times weaker than the peak intensity of the 1332-cm^{-1} line. One of the noteworthy features of the second-order spectrum is the sharp "line" at 2667 cm^{-1} (300°K) in contrast to all the other pronounced peaks. It is also evident from the figure that very little change occurs in the spectra when the temperature is lowered to ∼20°K. The clearly recognizable sharp features in Fig. 3 and 5–8 are labeled with encircled Arabic numbers; their existence has been established on the basis of several measurements of each spectrum reported. Features established to a lesser degree of reliability are indi-

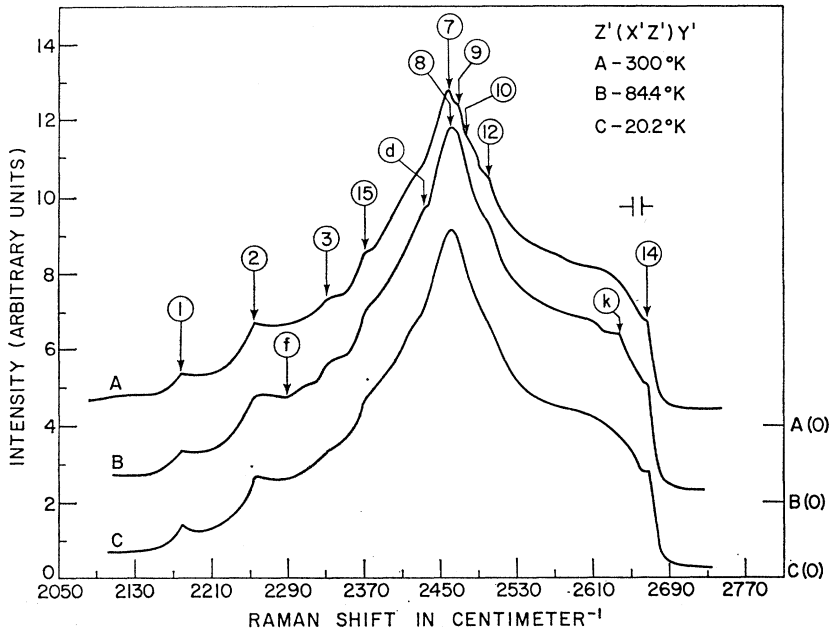

FIG. 5. Temperature dependence of the second-order Raman spectrum of diamond in the range 2050–2770 cm^{-1} for $Z'(X'Z')Y'$ scattering. The spectra were recorded with the 4880 Å radiation of the Ar^+ laser.

cated by encircled letters. Figure 4 compares the spectra for $I_{Z'(X'X')Y'}$ and $I_{Z'(X'Z')Y'}$ on the same scale; $I_{Z'(X'Z')Y'}$ is ~5–10 times weaker than $I_{Z'(X'X')Y'}$ throughout the entire range. The $I_{Z'(X'Z')Y'}$ spectrum recorded at 300, 84.4, and 20.2°K with a larger slit-width and higher amplification than in Fig. 4 is shown in Fig. 5. The most striking feature of this spectrum in comparison to $I_{Z'(X'X')Y'}$ is the absence of the sharp peak at 2667 cm^{-1}; i.e., the "sharp line" is highly polarized contrary to the behavior of the 1332 cm^{-1} line for this orientation. Figure 6 shows the $Z'(Y'X')Y'$ spectra recorded at the three temperatures indicated. The peak intensity of these spectra above the background is ~10^5 times less than that of the first-order line. The "line" at 2667 cm^{-1} is very weak in this spectrum. The $I_{Y'(Z'Z')X'}$ spectra shown in Fig. 7 are comparable in intensity to those of Fig. 3. For the crystallographic directions corresponding to X', Y', and Z', $I_{Y'(Z'Y')X'}=I_{Z'(X'Z')Y'}$ should hold. Experimentally, this has been verified in that the second-order spectrum

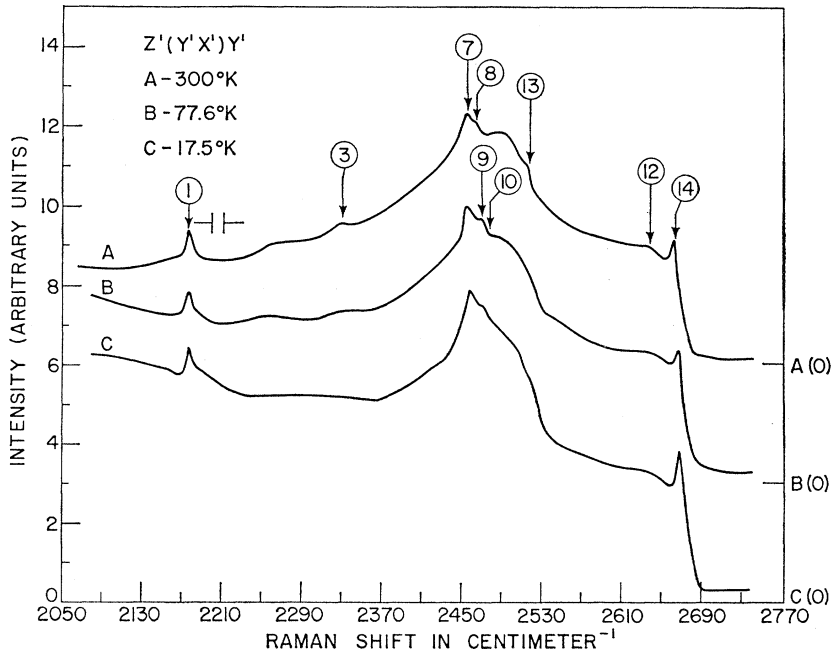

FIG. 6. Temperature dependence of the second-order Raman spectrum of diamond for $Z'(Y'X')Y'$ scattering in the range 2050–2770 cm^{-1}. The spectra were recorded with the 4880 Å radiation of the Ar^+ laser.

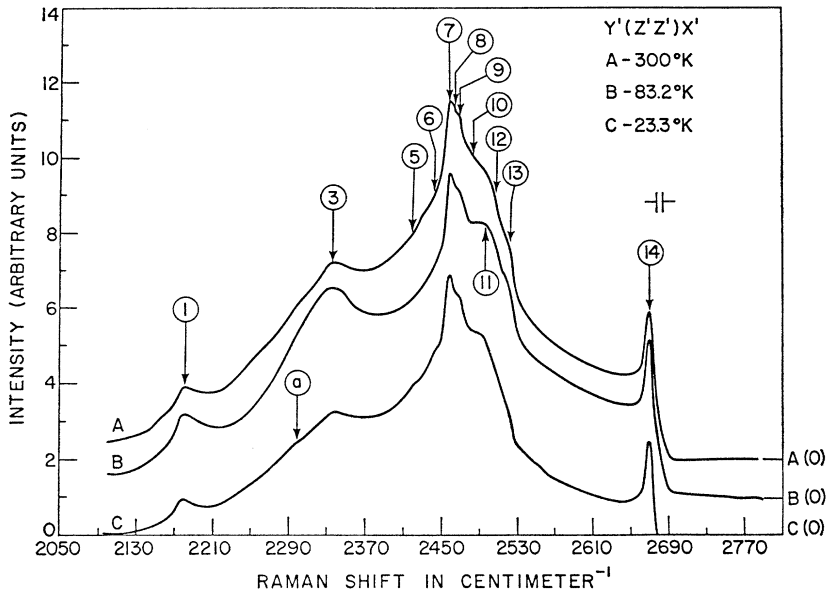

FIG. 7. Temperature dependence of the second-order Raman spectrum of diamond for $Y'(Z'Z')X'$ scattering in the range 2050–2770 cm^{-1}. The spectra were recorded with the 4880 Å radiation of the Ar^+ laser.

shown in Fig. 7 is found to be highly polarized in the direction of the electric vector of the incident light. It should be emphasized that the sharp line at 2667 cm^{-1} is found to be absent in both $Y'(Z'Y')X'$ and $Z'(X'Z')Y'$ in contrast to the behavior of the first-order line.

Since the second-order spectra should, in principle, appear in the range 0–2664 cm^{-1}, a careful search was made for Raman scattering in this region. Figure 8 shows a very weak quasicontinuous Raman scattering in the range 1600–2100 cm^{-1} for $Z'(X'X'+X'Z')Y'$ at the temperatures indicated. It was verified by exciting

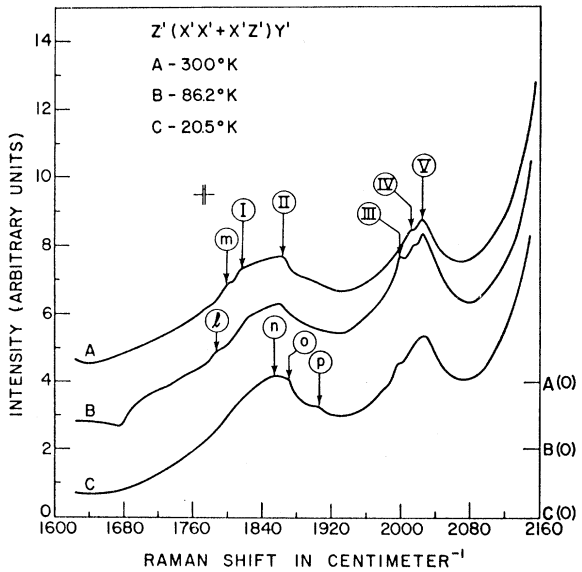

FIG. 8. Temperature dependence of the second-order Raman spectrum of diamond for $Z'(X'X'+X'Z')Y'$ scattering in the range 1600–2100 cm^{-1}. The spectra were recorded with the 4880 Å radiation of the Ar^+ laser.

the spectra with both 4880 and 5145 Å radiation that this is Raman scattering. The intensities of these spectra are $\sim 2.5\times 10^4$ weaker than the first-order Raman line. Individual measurements of $I_{Z'(X'X')Y'}$ and $I_{Z'(X'Z')Y'}$ revealed that the spectra are completely polarized, within the experimental limits of detection, in the direction of the incident electric vector. With the present experimental arrangement, measurements in the range 1300–1360 cm^{-1} were obscured by the intense first-order line whereas no scattering was observed between 100–1300 cm^{-1}. In Fig. 8, the reliable features have been labeled by encircled Roman numerals. In the observations reported by Krishnan[11] the presence of Hg lines at wavelengths other than 2537 Å obscured some features in the range 2330–2400 cm^{-1} as well as the new spectrum in the range 1600–2100 cm^{-1}. Attempts to observe third-order Raman scattering were not successful.

The five distinct processes which can give rise to second-order Raman scattering are listed in Table III. Also shown in the table are the temperature dependence and energy conservation governing each process. For second-order scattering in which phonons are created, processes II and IV need not be considered. Of the remaining, process V would predict orders of magnitude decrease in intensity in going from room temperature to liquid-helium temperature for the Raman spectrum in the range 1600–2800 cm^{-1}. As can be seen from Figs. 3 and 5–8 this is clearly not the case. On the other hand, processes I and III are comptabile with the observed temperature dependence. Hence, the interpretation of the second-order spectra will be made in terms of combinations and overtones.

We shall now attempt to interpret the observed second-order Raman spectrum in a manner consistent with conservation of wave vector and energy, critical

points as revealed by neutron-scattering data, and polarization characteristics consistent with selection rules. It is well known that for Raman scattering of visible radiation, wave-vector conservation requires the total wave vector of the phonons participating in the scattering process to be ~zero.[28] This restricts first-order Raman scattering to zone-center optical phonons. On the other hand, the two phonons of the second-order process must have equal and opposite wave vectors, a condition satisfied by many sets of phonons throughout the Brillouin zone. Thus, the second-order Raman spectrum should be a continuum rather than discrete lies.[29] The structure observed in the second-order Raman spectrum reflects the joint density of states deduced from the two-phonon dispersion curves; this assumes that the scattering cross section is a smooth function of the frequency shift.[28] Structure in the joint density of states arises from "critical points" in the two-phonon dispersion curves at which the gradient $\nabla_k\omega(k)$ is zero or discontinuous. In addition, for a critical point to manifest itself in the second-order Raman spectrum, the combination or overtone associated with that critical point must be Raman active. The selection rules can be deduced by a group theoretical analysis given by Birman.[30,31]

In the case of diamond, the polarizibility tensor transforms as $\Gamma^{(1+)}$, $\Gamma^{(12+)}$, or $\Gamma^{(25+)}$. Therefore, the reducible product and square representation corresponding to the combination and overtone, respectively, must contain one or more of these in order for it to be Raman-active. Further, the polarizibility tensor associated with each of the above representations will result in specific polarization features of the second-order Raman spectrum. The polarizibility tensors of $\Gamma^{(25+)}$ have been given in the discussion of the first-order Raman spectrum. The tensors for $\Gamma^{(1+)}$ and $\Gamma^{(12+)}$ with respect to $X'\|[110]$, $Y'\|[1\bar{1}0]$, $Z'\|[001]$ are given below:

$$\Gamma^{(1+)}: \begin{bmatrix} a & 0 & 0 \\ 0 & a & 0 \\ 0 & 0 & a \end{bmatrix},$$

$$\Gamma^{(12+)}: \begin{bmatrix} -b & 0 & 0 \\ 0 & -b & 0 \\ 0 & 0 & 2b \end{bmatrix} \quad \text{and} \quad \begin{bmatrix} 0 & -b\sqrt{3} & 0 \\ -b\sqrt{3} & 0 & 0 \\ 0 & 0 & 0 \end{bmatrix}.$$

Table IV shows the Raman-active representations which must appear in the product representation of a combination or an overtone in order for it to manifest itself in a given mode of obsrevation.

Let us first consider the sharp peak which appears with a shift of 2667 cm^{-1} at 300°K. From Fig. 4 it is evident that $I_{Z'(X'X')Y'} \gg I_{Z'(X'Z')Y'}$. By comparing the intensity of this line with respect to the 1332-cm^{-1} line observed under the same conditions and by taking into account the polarization feature of the latter it can be shown that $I_{Z'(X'X')Y'} \gg I_{Z'(Y'X')Y'}$. Thus, the 2667-cm^{-1} line has predominantly $\Gamma^{(1+)}$ symmetry. Loudon has suggested that sharp lines which appear in the second-order spectrum can be attributed to "two successive first-order Raman scatterings."[28] If the above line is due to photons scattered twice by the zone-center optical phonons of $\Gamma^{(25+)}$ symmetry, it should be depolarized for all directions of incidence and observation. The first scattering event results in Raman-scattered photons propagating in all directions in the crystal with polarization features determined by the direction of propagation. The second scattering event which produces twice scattered photons in the solid angle of observation will further scramble the polarization features. This is clearly not what is observed in the present measurements. In addition, the two-step process proposed by Loudon would be proportional to the square of the illuminated crystal volume whereas what is observed is a linear dependence on this volume.[32] It should also be noted that the Raman shift of this line is greater than

TABLE III. Temperature dependence of the second-order Raman spectrum.

Process	Description	Energy conservation[a]	Temperature dependence[b]
I	Create two phonons of equal energy	$\omega_s=\omega_i-2\omega_1$	$(n_1+1)(n_1+2)$
II	Destroy two phonons of equal energy	$\omega_s=\omega_i+2\omega_1$	$n_1(n_1-1)$
III	Create two phonons of different energy	$\omega_s=\omega_i-\omega_1-\omega_2$	$(n_1+1)(n_2+1)$
IV	Destroy two phonons of different energy	$\omega_s=\omega_i+\omega_1+\omega_2$	n_1n_2
V	Create one phonon and destroy one phonon of different energy	$\omega_s=\omega_i-\omega_1+\omega_2$	$n_2(n_1+1)$

[a] ω_i and ω_s are the frequencies of the incident and the scattered photons, respectively; ω_1 and ω_2 are the phonon frequencies.
[b] $n_j=[e^{\hbar\omega_j/kT}-1]^{-1}$, $j=1$ or 2.

TABLE IV. Dependence of Raman activity on polarization and crystal orientation.

Mode of observation	Raman-active representations
$Z'(X'X')Y'$	$\Gamma^{(1+)}$, $\Gamma^{(12+)}$, $\Gamma^{(25+)}$
$Z'(X'Z')Y'$	$\Gamma^{(12+)}$
$Z'(Y'X')Y'$	$\Gamma^{(12+)}$
$Y'(Z'Z')X'$	$\Gamma^{(1+)}$, $\Gamma^{(12+)}$

[29] For a discussion of the Raman-Born controversy and its relation to the second-order Raman spectrum of diamond, see Ref. 28, p. 466.
[30] J. L. Birman, Phys. Rev. **127**, 1093 (1962).
[31] J. L. Birman, Phys. Rev. **131**, 1489 (1963).
[32] Linear volume dependence was established from a comparison of $I_{Z'(X'X')Y'}$ with $I_{Y'(Z'Z')X'}$. In view of the Γ_1^+ symmetry of the 2667-cm^{-1} line such a comparison is valid.

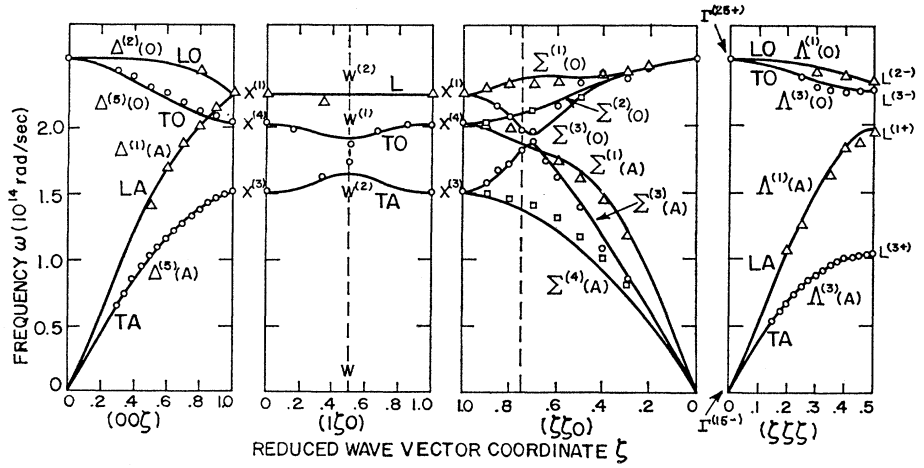

FIG. 9. Single-phonon dispersion curves of diamond deduced from neutron spectroscopic data at 296°K after Warren *et al.*, Phys. Rev. **158**, 805 (1966). The solid curves represent a shell-model fit to the data points. Branches and end points are labeled by (1) the phonon polarization vectors and (2) by the irreducible representation according to which they transform following Birman's notation in Ref. 30.

twice the shift of the first-order line, by ~ 2 cm^{-1} at 300°K and 2.5 cm^{-1} at liquid-nitrogen temperature and below. This feature is not expected from the "double" scattering process. Clearly the two-step process can only involve Raman lines active in the first order. In this context it is of interest to note that both cubic zinc blende[33] and gallium phosphide[34] show sharp lines in their second-order Raman spectra which involve phonons not active in the first-order Raman effect. If the 2667-cm^{-1} line of diamond is interpreted as an overtone, its symmetry will be $[\Gamma^{(25+)}]_{(2)}=\Gamma^{(1+)}+\Gamma^{(12+)}+\Gamma^{(25+)}$. The experimental measurements reported here are consistent with this interpretation provided the contribution from $\Gamma^{(1+)}$ dominates the scattering process. Since the joint density of states for diamond calculated by Dolling and Cowley[35] and Whener *et al.*[36] does not show a sharp peak corresponding to 2667 cm^{-1} the origin of this "line" cannot be regarded as settled. As remarked above the position of this line does not coincide exactly with the position of the overtone of the 1332-cm^{-1} line. It is well known that such effects may arise from mechanical anharmonicity.[37]

The critical points observed in both the Raman and infrared spectra will be analyzed using the following procedure: Assignments are made numerically by fitting the position of the observed critical point to the closest value of combination or overtone energy deduced from neutron data.[7] It should be pointed out that several critical points were found in the two-phonon dispersion curves along Σ which resulted from only one of the single phonon dispersion curves having a critical point. The symmetries of the phonons at various points in the

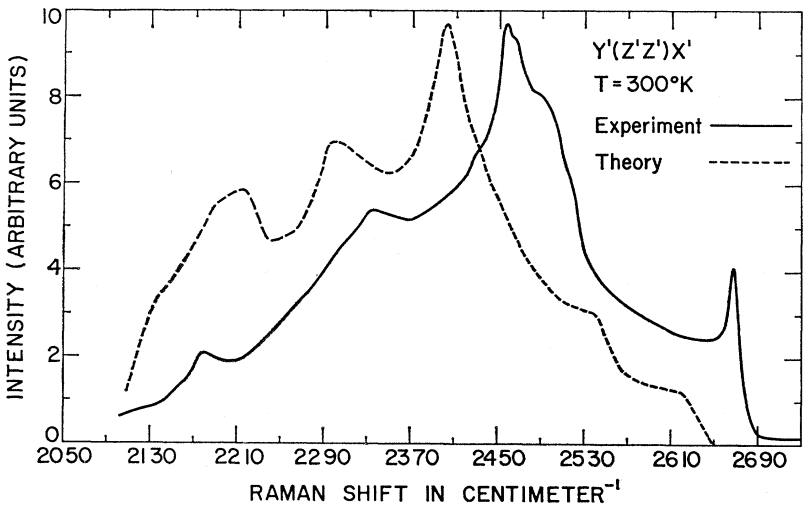

FIG. 10. Comparison of the theoretical calculation of Dolling and Cowley (Refs. 35 and 41) and the experimental results for the room-temperature second-order Raman scattering in diamond for $Y'(Z'Z')X'$. The strongest peak in their calculation has been normalized to the strongest peak in the experimental spectrum.

[33] W. G. Nilsen, Phys. Rev. **182**, 838 (1969).
[34] P. G. Marlow, J. P. Russell, and C. T. Sennett, Phys. Letters, **20**, 610 (1966).
[35] G. Dolling and R. A. Cowley, Proc. Phys. Soc. (London) **88**, 463 (1966).
[36] See Ref. 4 where the authors use a different value of the second-neighbor parameter δ, compared to that used in Ref. 35.
[37] See, for example, E. B. Wilson Jr., J. C. Decius, and P. C. Cross, *Molecular Vibrations* (McGraw-Hill Book Co., New York, 1955), p. 193.

Brillouin zone are given in Fig. 9 which shows the experimental and theoretical dispersion curves of diamond obtained by Warren *et al.*[7] Assignments were further restricted on the basis of limitations demanded by infrared activity and Raman activity (see Table V); for the latter, polarization features were taken into account. On the basis of the above analysis, it was possible to identify most of the reproducible features observed in the Raman and infrared spectra. It was ensured that the single-phonon energies including their error deduced from the two-phonon assignments lie within the error brackets of the neutron-scattering assignment for that particular phonon.

A summary of the analysis described above is given in Table VI. The polarization properties of the Raman spectra and the selection rule with respect to infrared activity are also included. The + (−) occurring under the subcolumn "Th" indicated that the critical point associated with it should (not) appear in the measurement described in the column heading. Similarly, the + (−) occurring under the subcolumn "Exp" indicates that the critical point was (not) experimentally observed. Note that "Th(+) Exp(−)" is not necessarily a contradiction while "Th(−) Exp(+)" is definitely one. The values given in the table are for room temperature measurements. In the column labeled "calculated," the positions of the critical points in the second-order spectra are compared with those deduced from neutron data and the phonon assignments based on optical data. The single-phonon energies deduced from the two-phonon critical-point assignments of Table VI are listed in Table VII for the Γ, X, L, W, and Σ points of the Brillouin zone. The typical error in the phonon energies of Table VII deduced from optical data is 0.5%; nevertheless, the values listed are considerably more accurate than those deduced from neutron spectroscopy, the latter having errors of the order of ±3%.

As a check on phonon energies and assignments, it is of interest to calculate the sum $\sum_{i=1}^{3n}\tilde{\nu}_i^2(\mathbf{q})$ for the points in the Brillouin zone for which the phonon energies have been deduced above from optical data; here n is the number of atoms per primitive cell, $\tilde{\nu}$ is the phonon wave number and $\mathbf{q}$ is the wave vector. For diamond, $n=2$ and the sum is over the six branches in the phonon dispersion curve. This sum is shown in Table VII under the column "Brout sum." The importance of such a sum was pointed out by Brout[38] and discussed in detail by Rosenstock.[39] Brout showed that the above sum is a constant independent of $\mathbf{q}$ for ionic lattices of tetrahedral symmetry having two atoms per primitive cell, whereas Rosenstock demonstrated that the sum is also a constant for crystals in which the interatomic forces are electrostatic and/or act between inequivalent atoms. It is clear from Table VII that the Brout sum calculated for diamond is not independent of $\mathbf{q}$; it shows a variation as large as 17%, which is well outside the 1–2% experimental error introduced by the ±5-cm^{-1} error in the phonon assignments. In contrast, the Brout sum is a constant for the analogous cases of silicon and germanium as shown by Rosenstock[39] using neutron data. This is not surprising, since it is known that silicon and germanium though homologous to each other, are not so to diamond. Rosenstock[39] and Bilz *et al.*[10] attributed this $\mathbf{q}$ dependence of the Brout sum in diamond to central second-neighbor forces. The present results can also be interpreted similarly.

Dolling and Cowley[35,41] have calculated the intensity distribution of the second-order Raman spectrum of diamond taking into account the direction and polariza-

TABLE V. Reduction coefficients corresponding to Raman- and infrared-active representations of overtones and combinations.

Combinations or overtones	Raman-active $\Gamma^{(1+)}$	$\Gamma^{(12+)}$	$\Gamma^{(25+)}$	Infrared-active $\Gamma^{(15-)}$
$[\Gamma^{(25+)}]_{(2)}$	1	1	1	0
$[{}^*X^{(1)}]_{(2)}$	1	1	1	0
$[{}^*X^{(2)}]_{(2)}$	1	1	1	0
$[{}^*X^{(3)}]_{(2)}$	1	1	1	0
$[{}^*X^{(4)}]_{(2)}$	1	1	1	0
${}^*X^{(1)}\otimes{}^*X^{(2)}$	0	1	0	1
${}^*X^{(1)}\otimes{}^*X^{(3)}$	0	0	1	1
${}^*X^{(1)}\otimes{}^*X^{(4)}$	0	0	1	1
${}^*X^{(2)}\otimes{}^*X^{(3)}$	0	0	1	1
${}^*X^{(2)}\otimes{}^*X^{(4)}$	0	0	1	1
${}^*X^{(3)}\otimes{}^*X^{(4)}$	0	1	0	1
$[{}^*L^{(1+)}]_{(2)}$	1	0	1	0
$[{}^*L^{(2-)}]_{(2)}$	1	0	1	0
$[{}^*L^{(3+)}]_{(2)}$	1	1	2	0
$[{}^*L^{(3-)}]_{(2)}$	1	1	2	0
${}^*L^{(1+)}\otimes{}^*L^{(2-)}$	0	0	0	1
${}^*L^{(1+)}\otimes{}^*L^{(3+)}$	0	1	1	0
${}^*L^{(1+)}\otimes{}^*L^{(3-)}$	0	0	0	1
${}^*L^{(2-)}\otimes{}^*L^{(3+)}$	0	0	0	1
${}^*L^{(2-)}\otimes{}^*L^{(3-)}$	0	1	1	0
${}^*L^{(3+)}\otimes{}^*L^{(3-)}$	0	0	0	2
$[{}^*W^{(1)}]_{(2)}$	1	1	1	0
$[{}^*W^{(2)}]_{(2)}$	1	1	1	0
${}^*W^{(1)}\otimes{}^*W^{(2)}$	0	1	2	2
${}^*W^{(2)}\otimes{}^*W^{(2)}$	1	1	1	1
$[{}^*\Sigma^{(1)}]_{(2)}$	1	1	1	0
$[{}^*\Sigma^{(2)}]_{(2)}$	1	1	1	0
$[{}^*\Sigma^{(3)}]_{(2)}$	1	1	1	0
${}^*\Sigma^{(1)}\otimes{}^*\Sigma^{(2)}$	0	0	1	0
${}^*\Sigma^{(1)}\otimes{}^*\Sigma^{(3)}$	0	0	1	1
${}^*\Sigma^{(1)}\otimes{}^*\Sigma^{(4)}$	0	1	0	1
${}^*\Sigma^{(2)}\otimes{}^*\Sigma^{(3)}$	0	1	0	1
${}^*\Sigma^{(1)}\otimes{}^*\Sigma^{(1)}$	1	1	1	1
${}^*\Sigma^{(2)}\otimes{}^*\Sigma^{(2)}$	1	1	1	1
${}^*\Sigma^{(3)}\otimes{}^*\Sigma^{(3)}$	1	1	1	1

[38] R. Brout, Phys. Rev. **113**, 43 (1959).
[39] H. B. Rosenstock, in *Lattice Dynamics*, edited by R. F. Wallis (Pergamon Press, Ltd., London 1965), p. 205.
[40] J. L. Yarnell, J. L. Warren, and R. G. Wenzel, Phys. Rev. Letters **13**, 13 (1964).
[41] Our special thanks are due to Dr. R. A. Cowley who supplied us with the details of the calculations necessary for the construction of Fig. 10.

TABLE VI. Assignments for the second-order Raman and infrared spectrum of diamond.

Serial[a] No.	Raman (cm^{-1})	Infrared[b] (cm^{-1})	Assignment[c]	Calculated (cm^{-1}) neutron[c]	optical[c]	Raman activity $Z'(X'X')Y'$ Th	Exp	$Y'(Z'Z')X'$ Th	Exp	$Z'(X'Z')Y'$ Th	Exp	$Z'(Y'X')Y'$ Th	Exp	Infrared activity Th	Exp
		1815	$LO(L^{(2-)})+TA(L^{(3+)})$	1799±56	1815	−	−	−	−	−	?	−	?	+	+
I	1817		$2TA(W^{(2)})$	1836±22	1816	+	+	+	+	+	?	+	?	−	−
II	1864	1871	$TA(X^{(3)})+TO(X^{(4)})$	1879±58	1876	+	+	+	+	+	?	+	?	+	+
		1968	$\Sigma^{(1)}(A)+\Sigma^{(3)}(A)$	1975±40	1976	+	−	−	−	+	?	−	?	+	+
		1992	$L(X^{(1)})+TA(X^{(3)})$	1991±53	1992	+	−	−	−	+	?	−	?	+	+
III	1998		$2TO(W^{(1)})$	1986±106	1998	+	+	+	+	+	?	+	?	−	−
IV	2011		$2LA(L^{(1+)})$	2070±64	2012	+	+	+	+	+	?	−	?	−	−
V	2025	2025	$\Sigma^{(3)}(0)+\Sigma^{(3)}(A)$	2039±37	2025	+	+	+	+	+	?	+	?	+	+
		2041	$\Sigma^{(3)}(0)+\Sigma^{(1)}(A)$	2028±32	2041	+	−	−	−	+	?	−	?	+	+
		2081	$\Sigma^{(2)}(0)+\Sigma^{(3)}(A)$	2113±56	2089	+	−	+	−	−	−	+	−	+	+
		2113	$\Sigma^{(3)}(0)+\Sigma^{(1)}(A)$[d]	2086±88		+	−	−	−	+	−	−	−	+	+
		2154	$\Sigma^{(2)}(0)+\Sigma^{(3)}(0)$	2166±48	2154	+	−	+	−	−	−	+	−	+	+
1	2177	2178	$L(W^{(2)})+TO(W^{(1)})$	2161±106	2178	+	+	+	+	+	+	+	+	+	+
		2210	$\Sigma^{(1)}(0)+\Sigma^{(3)}(A)$	2224±48	2210	+	−	−	−	+	−	−	−	+	+
2	2254		$L(X^{(1)})+TO(X^{(4)})$	2256±47	2254	+	+	−	−	+	+	−	−	+	−
		2267	$LA(L^{(1+)})+LO(L^{(2-)})$	2275±72	2258	−	−	−	−	−	−	−	−	+	+
3	2333	2331					+		+		+		+		+
		2355					−		−		−		−		+
15	2370		$2L(X^{(1)})$	2371±40	2370	+	−	+	−	+	+	+	−	−	−
5	2422		$2TO(L^{(3-)}$	2420±74	2412	+	−	+	+	+	−	+	−	−	−
		2436					−		−		−		−		+
7	2458		$TO(L^{(3-)})+LO(L^{(2-)})$	2452±72	2458	+	+	+	+	+	+	+	+	−	−
8	2461		$2\Sigma^{(1)}(0)$	2461±64	2460	+	+	+	+	+	+	+	+	−	−
9	2467						+		+		?		?		−
10	2485						+		+		+		+		−
12	2054		$2LO(L^{(2-)})$	2484±72	2504	+	+	+	+	+	+	−	−	−	−
13	2519						+		+		+		+		−
14	2667		$2O(\Gamma^{(25+)})$	2665±1	2665	+	+	+	+	+	+	+	+	−	−

[a] The serial numbers refer to Figs. 3 and 5–8.
[b] With the exception of the kinks at 1871, 2331, and 2355 cm^{-1}, all the values in this column are from Ref. 3; the former are from Ref. 4.
[c] The phonons are labeled here by the type and the irreducible representation as shown in Fig. 9; the notation for the latter follows Birman (Refs. 30 and 31).
[d] This corresponds to $(q/q_{max})\sim 0.5$, where q is the wave vector of the phonon.
[e] Calculated from the phonon energies chosen from neutron data and optical data as given in Table VII.

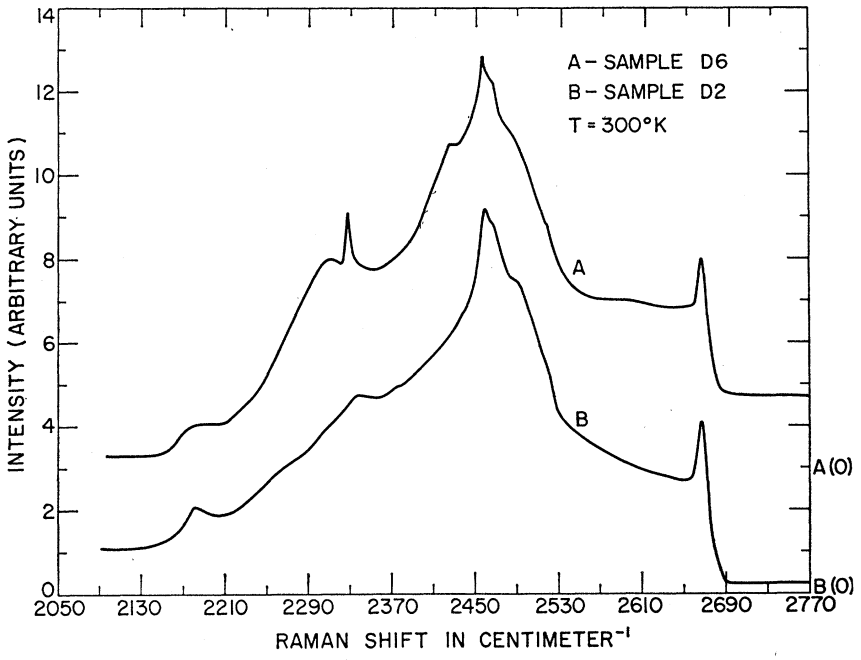

FIG. 11. Comparison of the second-order Raman spectra of a type-I (curve *A*) and type-IIb (curve *B*) diamond for scattering in the 2050–2770-cm^{-1} range. Both spectra were excited with the 5145 Å radiation of the Ar^+ laser incident along a ⟨111⟩ direction. The relative intensity scales of the two spectra are not correlated in the figure. The spectrum labeled *A* was superimposed on a large luminescence background not shown in the figure.

tion of the incident and scattered beam with respect to sample orientation. A comparison of their calculations[35] for $I_{Z(XX)Y}$ with our experimental observations of $I_{Y'(Z'Z')X'}$ is shown in Fig. 10; note $I_{Z(XX)Y}=I_{Y'(Z'Z')X'}$, X, Y, and Z being the cubic directions. In view of the approximations made in their shell-model calculations, the agreement between theory and experiment is reasonably good. Clearly it is of interest to compare calculations which include second and more-distant neighbors with the experimental results. The interpretation for the line at 2667 cm^{-1} in the calculations of Dolling and Cowley is based on Loudon's suggestion of multiple scattering. However, as discussed earlier, this interpretation is not consistent with experimental observation; hence, the calculated curve in Fig. 10 does not include the contribution due to this peak.

IV. CONCLUDING REMARKS

The assignments in Table VI for the critical points observed in the second-order Raman and infrared spectra were based on an analysis in which an equal weight was given to all the reliable features. However, for such an analysis to be considered successful all the prominent features must be explained; in the second-order Raman spectra shown in Figs. 4–9, 1, 2, 3, 7, and 14 are examples of such features. In this context, attention should be drawn to the feature labeled 3 which occurs at 2333 cm^{-1} in the Raman spectrum and at 2331 cm^{-1} in the infrared; it was not possible to account for this in the above analysis. It was also noticed that this feature was unique in that its shape depended on the type of diamond examined. A comparison of the second-order Raman spectrum of a type-I and a type-IIb diamond is shown in Fig. 11; both spectra were excited by light incident along a ⟨111⟩ direction. In the former, a sharp peak occurs close to 2333 cm^{-1}, viz., at 2329 cm^{-1} in contrast to the "kink" observed at this position in the latter. The spectrum labeled *A* is superimposed on a large luminescence background. None of the type-IIb or type-IIa samples examined showed the sharp line at 2329 cm^{-1}, while the two type-I specimens for which it was possible to obtain the second-order Raman spectrum did show it. It is well known[42] that type-I diamonds in contrast to

TABLE VII. Summary of phonon energies at high-symmetry points of the Brillouin zone.

Symmetry point	Phonon	Energy (cm^{-1}) Neutron	Optical[a]	"Brout sum" (from optical data) (10^6 cm^{-2})
Γ	0		1332±0.5	5.322
X	TO	1072±26	1069	6.396
	L	1184±21	1185	
	TA	807±32	807	
L	TO	1210±37	1206	6.122
	LO	1242±37	1252	
	TA	552±16	563	
	LA	1035±32	1006	
W	TO	993±53	999	6.426
	L	1168±53	1179	
	TA	918±11	908	
$\Sigma(q/q_{max}\sim0.7)$[b]	$\Sigma^{(1)}(0)$	1231±32	1230	6.331±0.024
	$\Sigma^{(2)}(0)$	1120±21	1109	
	$\Sigma^{(3)}(0)$	1046±21	1045	
	$\Sigma^{(1)}(A)$	982±11	988	
	$\Sigma^{(3)}(A)$	993±16	980	
	$\Sigma^{(4)}(A)$	748±16		

[a] Error in these numbers is ±5 cm^{-1} except as noted.
[b] Only $\Sigma_1(0)$, $\Sigma_3(0)$, and $\Sigma_3(A)$ show critical points in the one-phonon dispersion curves (see Fig. 9). Note: The value of $\Sigma^{(4)}(A)$ was not determined from optical data.

[42] W. Kaiser and W. L. Bond, Phys. Rev. **115**, 857 (1959).

type II contain considerable quantities of nitrogen. At this stage it is not clear whether this line is due to a local mode, an electronic transition or a two-phonon combination activated by the nitrogen impurities. In this connection it is interesting to note that the combination $\Sigma^{(1)}(0)+\Sigma^{(2)}(0)$ at 2339 cm^{-1} is close to 2333 cm^{-1}; however, the former is Raman-active in $Z'(X'X')Y'$ and $Y'(Z'Z')X'$, Raman-inactive in $Z'(X'Z')Y'$ and $Z'(Y'X')Y'$ and inactive in the infrared, whereas the 2333-cm^{-1} feature appears in all of these (see Table VI). Therefore, $\Sigma^{(1)}(0)+\Sigma^{(2)}(0)$ taken together with a relaxation of the selection rules caused by the nitrogen impurities may account for the feature at 2333 cm^{-1}.

Johnson and Loudon[9] and Bilz *et al.*[10] have discussed the shape and topological features of the critical points in the second-order spectra of silicon, germanium, and diamond. It appears that the experimentally observed features in the second-order Raman spectrum of diamond are not amenable to such analysis. Modulation techniques[43] such as those used in the analogous problems of the critical points in the optical-reflection spectra of semiconductors might be usefully applied to the study of the second-order Raman and infrared spectra.

ACKNOWLEDGMENTS

The authors wish to express their appreciation to Professor Peter Fisher and Professor Sergio Rodriguez for stimulating discussions and comments, and to Professor H. J. Yearian who oriented some of the diamond crystals used in this study.

[43] B. O. Seraphin and N. Bottka, Phys. Rev. Letters **15**, 104 (1965); G. Ascarelli and A. Barone, Nuovo Cimento **37**, 818 (1965); G. Ascarelli, Phys. Rev. **179**, 797 (1969); G. W. Gobeli and E. O. Kane, Phys. Rev. Letters **15**, 142 (1965); and W. E. Engler, H. Fritzsche, M. Garfinkel, and J. J. Tiemann, *ibid.* **14**, 1069 (1965).

PHYSICAL REVIEW B VOLUME 1, NUMBER 4 15 FEBRUARY 1970

Semiempirical Calculations of Ionic Polarizabilities and van der Waals Potential Coefficients for the Alkaline-Earth Chalcogenides*

I. M. Boswarva†
Metallurgy Department, Imperial College, London, England
(Received 28 July 1969)

Electronic polarizabilities for the ions of the alkaline-earth chalcogenides have been calculated by assuming an additivity law within the family of salts and a Lorentz factor of $\frac{4}{3}\pi$, and using experimental refractive indices and interionic distances. It is shown that the additivity assumption is well obeyed, and the Lorentz factor value of $\frac{4}{3}\pi$ gives the best fit to the data. Each polarizability obtained has been related to a mean excitation or characteristic energy for the ion, and hence the coefficients of the dipole-dipole and dipole-quadrupole terms of the van der Waals interaction energy derived.

1. INTRODUCTION

TWO approaches to the evaluation of the polarizabilities of ions in ionic crystals are well established. The first, pioneered by Tessman, Kahn, and Shockley[1] (hereafter referred to as TKS) and recently extended by Pirenne and Kartheuser[2] and Kartheuser and Naylor[3] assumes that within a family of salts the electronic polarizability of each substance is the sum of the electronic polarizabilities of the individual ions and that each ion polarizability is constant within the family. Under the further assumption that the electrostatic interactions between ions are purely of the dipole-dipole type the effective field acting on an ion $E_{\text{eff}}=E+LP$, where E is the externally applied field, P is the electronic polarization and the Lorentz factor, L, has a value of $\frac{4}{3}\pi$. The polarizability per ion pair α_m is then related to the refractive index of the salt, n, through the Clausius-Massotti relation

$$\alpha_m=(3V_m/4\pi)(n^2-1)/(n^2+2), \qquad (1)$$

where V_m is the volume occupied by an ion pair. The ion polarizabilities α_i are chosen to attain a best fit to α_m values throughout the family and the achievement of such a fit is taken as a measure of the validity of the assumptions.

All the previous workers have considered the alkali halides, although TKS have derived the only previously reported values of alkaline-earth ion polarizabilities by substracting their halide values from the ion-pair polarizabilities of the alkaline-earth halides. With these alkaline-earth values, a further step to the alkaline-earth chalcogenide family gives chalcogenide values, as does a study of the alkali chalcogenides. Such a process implies the dubious extension of the concept of constancy of an ion polarizability within one family to

* Work performed under contract at the National Bureau of Standards, 1967.
† Contribution of the National Bureau of Standards, not subject to copyright.
[1] J. R. Tessman, A. H. Kahn, and W. Shockley, Phys. Rev. **92**, 890 (1953).
[2] J. Pirenne and K. Kartheuser, Physica **30**, 2005 (1964).
[3] K. Kartheuser and K. A. Naylor, Phys. Letters **19**, 548 (1966).